Colloids and Surfaces B: Biointerfaces 154 (2017) 123–132

Contents lists available at ScienceDirect

Colloids and Surfaces B: Biointerfaces

journal homepage: www.elsevier.com/locate/colsurfb

Protocols

Design, characterization and *in vitro* evaluation of linalool-loaded solid lipid nanoparticles as potent tool in cancer therapy

Boris Rodenak-Kladniew[a], German A. Islan[b], Margarita G. de Bravo[a], Nelson Durán[c,d], Guillermo R. Castro[b,*]

[a] *Instituto de Investigaciones Bioquímicas de La Plata (INIBIOLP), CONICET-UNLP, CCT-La Plata, Facultad de Ciencias Médicas, La Plata, Argentina*
[b] *Laboratorio de Nanobiomateriales, CINDEFI, Departamento de Química, Facultad de Ciencias Exactas, Universidad Nacional de La Plata-CONICET (CCT La Plata), Calle 47 y 115., C.P. 1900 La Plata, Argentina*
[c] *Institute of Chemistry, Biological Chemistry Laboratory, Universidade Estadual de Campinas, C.P. 6159, CEP 13083-970 Campinas, SP, Brazil*
[d] *Brazilian Nanotechnology National Laboratory (LNNano-CNPEM), Campinas, SP, Brazil*

ARTICLE INFO

Article history:
Received 18 October 2016
Received in revised form 2 March 2017
Accepted 7 March 2017
Available online 9 March 2017

Keywords:
Linalool solid lipid nanoparticles
Cytotoxicity
Drug delivery
Cancer cells
Cellular uptake

ABSTRACT

Linalool (LN) is a monoterpene found in essential oils of plants and herbs that produces multiple effects on the mevalonate pathway and interesting antiproliferative activity in cancer cells. However, due to its poor aqueous solubility, an efficient vehicle is needed to improve its administration and bioavailability in physiological media.

LN encapsulation in solid lipid nanoparticles (SLN) with different compositions was explored and *in vitro* tested in two cancer cell lines. SLN of myristyl myristate (MM), cetyl esters (SS) and cetyl palmitate (CP) were prepared by sonication in the presence of Pluronic® F68 as surfactant. Nanoparticle size, morphology and distribution were determined by dynamic light scattering in combination with optical and transmission electron microscopy (TEM). SLN showed spherical shape and mean diameters in the range of 90–130 nm with narrow size dispersion (PDI values lower than 0.2) and Z potentials around −4.0 mV. The encapsulation percentages of LN in SLN were higher than 80% for all tested formulations and exhibited *in vitro* LN controlled release profiles for at least 72 h. The nanoparticles were physicochemically characterized by FTIR, XRD, DSC and TGA, and the incorporation of LN into SLN was higher than 80% in tested matrices. The developed formulations, and in particular SLN (MM)-LN, showed *in vitro* antiproliferative effects on hepatocarcinoma (HepG2) and lung adenocarcinoma (A549) cell lines in a dose-dependent response, and higher inhibitory effects were found in comparison with free LN. The cellular uptake of SLN was demonstrated by fluorescence microscopy, enhancing the ability of nanoparticles to intracellularly deliver the cargo molecules.

1. Introduction

Nowadays, cancer is the second leading cause of death in the world after cardiovascular diseases. Cancer is a complex disease characterized by the accumulation of mutations that lead to a sustained proliferation of cells capable of evading different physiological control mechanisms. It was responsible for 8.2 million deaths per year in 2012 and 11.4 million cancer deaths are predicted for 2030. Among the most common causes of cancer death, lung (1.59 million) and liver (745,000) are the two most frequent [1]. For that reason, there is an increasing interest in the discovery and development of novel alternatives and more effective therapies.

In the last few years, the use of natural compounds has been rediscovered, and more than 60% of the currently used anticancer drugs are, or are derived from, natural compounds [2]. The therapeutic potential of phytochemicals becomes an interesting alternative since the commercially available cancer drugs tend to show high systemic toxic effects due to many factors such as high dispersion in the body, high toxicity, low bioavailability, lack of drug concentration in the range of the therapeutic window associated in some cases with high dispersion of the drug in the body, and absence of drug controlled release delivery devices. Interestingly, phytochemicals have emerged as inexpensive and potent selective cytotoxic agents in cancer cells with minimum alteration of normal cells [3,4].

* Corresponding author.
E-mail addresses: grcastro@gmail.com, grcastro@quimica.unlp.edu.ar (G.R. Castro).

http://dx.doi.org/10.1016/j.colsurfb.2017.03.021
0927-7765/

In particular, linalool (3,7-dimethyl-1,6-octadien-3-ol) is an acyclic monoterpene alcohol commonly found in essential oils of more than 200 species of plants and herbs including lavender, basil, rosemary, citric fruits, green and black tea, among others. This natural isoprenoid is widely used in cosmetics and in the food industry as a fragrance and flavor agent, respectively, with an annual world consumption higher than 1000 m^3 [5,6]. In addition, several reports evidence the pharmacological properties of linalool both *in vivo* and *in vitro* as sedative, anxiolytic, analgesic, anesthetic, anti-inflammatory [7], antioxidant [8], neuroprotective [9], antimicrobial [10], and antitumor agent. In this sense, linalool could be used as a mono-drug agent [4,11,12] or combined with traditional drugs to potentiate the anticancer effects [13].

Despite their proven chemopreventive and chemotherapeutic efficiency, monoterpenes show poor water solubility, high volatility and require relatively elevated doses to fit inside the therapeutic window, which has limited their use in regular therapies. Some solubilizing agents, such as dimethyl sulfoxide (DMSO), usually improve their bioavailability but can also elicit cell toxicity, and harmful undesirable side effects can be found after prolonged exposure [14].

To overcome these drawbacks, several drug delivery systems have been proposed [15]. Among them, solid lipid nanoparticles (SLN) are colloidal carrier systems widely use since the 1990s for the encapsulation of lipophilic compounds as an alternative to traditional colloidal carriers, such as emulsions, liposomes and polymeric nanoparticles [16,17]. The main advantages of SLN include a good physical stability, controlled drug release profile, surface modification ability/capability in order to improve cell-targeting, and protection of drugs from environmental degradation. Also, they are nontoxic, biocompatible, and can be prepared at laboratory or large scale [18–20]. The SLN can be designed for oral, transdermal and intravenous administrations with the advantage that their particular structure favors their intratumoral accumulation [16]. It was demonstrated that the encapsulation of LN in a nanostructured lipid carrier improves the pharmacokinetic parameters and increases its bioavailability compared with the free drug [15].

The aim of the present study is the design of linalool-loaded SLN composed of different lipids, *i.e.*, myristyl myristate, cetyl esters or cetyl palmitate, in order to obtain high encapsulation efficiencies, a controlled release profile of LN, narrow size particle distribution and stability during storage. The SLN were characterized by biophysical methods (TEM, DLS, FTIR, XRD, TGA, DSC), and the antitumoral activity of the developed formulations was tested against human lung- and liver-derived tumor cell lines.

2. Materials and methods

2.1. Materials

The lipids myristyl myristate, cetyl esters and cetyl palmitate (Crodamol™ MM, SS, and CP, respectively) were kindly donated by Croda (Argentina). Linalool (purity > 95%), 3-(4,5-dimethylthiazol-2-yl)-2,5-diphenyltetrazolium bromide (MTT), Pluronic® F68, and 3,3′-dioctadecyloxacarbocyanine perchlorate (DiOC18) were provided by Sigma–Aldrich (Buenos Aires, Argentina). Other reagents were of analytical grade from available commercial sources and used as received from Merck (Darmstadt, Germany) or similar brand.

2.2. Preparation of solid lipid nanoparticles

SLN containing linalool (LN) were prepared by sonication [21]. Briefly, 400 mg of lipids (2.0%, w/v) was melted in a water bath at 60–70° C and mixed with 500 μl of LN. After 10 min, a hot aqueous solution (20 ml) containing 3.0% (w/v) of Pluronic® F68 was added to the lipid phase. Immediately, the mixture was sonicated for 30 min (50% amplitude) using an ultrasonic processor (130 W, Cole-Parmer, USA) equipped with a 6 mm titanium tip. Then, the dispersion was cooled at room temperature and stored at 5 °C.

2.3. LN detection

Linalool detection was performed by UV–vis spectroscopy. Two wavelengths at λ_{max1} = 233 nm (intense, but with interference) and λ_{max2} = 275 nm (weak, but stable) were found. LN calibration curves were performed in the range from 1.0 to 30.0 mg/ml dissolved in 90% ethanol at the two selected wavelengths (Fig. S1).

2.4. Measurement of loading efficiency

The volume of the formulation was measured after finishing the preparation, and the concentration of free LN was determined. Briefly, samples of 500 μl were transferred to an ultrafiltration centrifugal device (MWCO 10,000, Microcon, Millipore, MA, USA) and centrifuged at 5000 × g at 5 °C for 10 min. The filtrate was ten times diluted in ethanol and the non-encapsulated LN was measured by UV–vis spectroscopy (λ_{max} = 275 nm). The encapsulation efficiency (EE) was calculated as follows:

$$EE\,(\%) = \frac{(Q_0 - (Cr \times V))\,X\,100}{Q_0} \quad (1)$$

where Q_0 is the initial amount of LN, Cr is concentration of LN in the filtered solution, and V is the final volume after preparation.

2.5. Particle size, zeta potential (Z pot) and polydispersity index (PDI)

The mean diameter and size distribution were measured by photon correlation spectroscopy (Nano ZS Zetasizer, Malvern Instruments Corp., UK) at 25 °C in polystyrene cuvettes with a path length of 10 mm. The zeta potential was determined by laser Doppler anemometry also using the Nano ZS Zetasizer. Measurements were performed in capillary cells with path lengths of 10 mm, using deionized water obtained from a Milli-Q system. Also the PDI value was determined. All the measurements were carried out in triplicate.

2.6. Physical stability

The physical stability of the nanoparticle dispersion was evaluated by examining changes in mean particle size, Z pot, PDI and EE during storage at 4 °C and protected from light.

2.7. Release studies

Molecular release experiments were performed using a dialysis membrane (MWCO 10 kDa, Spectra Pore, USA). The membrane was soaked in distilled water for 24 h and filled with 3.0 ml of each formulation (LN loaded SLN: MM, SS and CP) followed by incubation in 30 ml of 10 mM phosphate buffer (pH 7.4) with 10% (v/v) ethanol at 37 °C and 150 rpm [22,23]. Every 1 h, samples of 10 ml were withdrawn, and LN concentration was measured at 275 nm using a UV–vis spectrophotometer (Shimadzu, Japan). Then, the vial was replenished with 10 ml of fresh media to keep a constant release volume.

2.8. Microscopic studies

2.8.1. Optical microscopy (OM)

Optical microscopy observations of the nanoparticles were performed in a Leica DM 2500 microscope (Germany).

2.8.2. Transmission electron microscopy (TEM)

The nanoparticle dispersion was ten times diluted with ultrapure water, and a drop of the dispersion was spread onto a collodion-coated Cu grid (400-mesh). Liquid excess was drained with filter paper, and for contrast enhancement a drop of phosphotungstic acid was added to the SLN dispersion. Finally, TEM analysis was performed using Jeol-1200 EX II-TEM microscope (Jeol, MA, USA).

2.9. Fourier transformed infrared spectroscopy (FTIR)

The FTIR spectra of the samples were scanned in the range of 450–4000 cm^{-1} at a resolution of 2 cm^{-1} (JASCO FT/IR- 4200 spectrometer) with background correction at 256 number scans, against a high energy ceramic source and DLATGS detector. Pellets were prepared by mixing the samples at 5% (w/w) with potassium bromide (KBr, Pike Technologies).

2.10. Differential scanning calorimetry (DSC) analysis

The thermal properties of linalool, SLN-CP, SLN-SS, SLN-MM and LN-loaded nanoparticles were determined by differential scanning calorimetry (DSC Q100 V9.9 Build 303) under nitrogen atmosphere. Scans were carried out at a heating rate of 10 °C min^{-1} in the temperature range from 0 °C to 250 °C (modulate mode).

2.11. Thermo-gravimetric analysis (TGA)

TGA was conducted to study the thermal stability of linalool, SLN-CP, SLN-SS, SLN-MM and LN loaded nanoparticles. TGA data were obtained using a thermo-gravimetric analyzer (TGA-50 Shimadzu, Japan). Samples of 5.0–10.0 mg were accurately weighed in aluminium pans, and the TGA measurements were conducted at a heating rate of 10 °C min^{-1} under nitrogen atmosphere.

2.12. X-ray diffraction (XRD)

X-ray diffraction patterns were taken on PANalytical X'Pert PRO diffractometer equipped with an X-ray source (Philips PW 1830, PANalytical BV, the Netherlands) using CuKα radiation at 40 kV and 40 mA. Diffraction patterns were collected over the 2θ range of 5°–75° with an acquisition time of 1 s at each step of 0.02°. Scattering angles were transformed into short spacings using Bragg's equation: 2d (equipped with X-ray source (Philips PW 1830, PANalytical BV) using CuK measurement.

2.13. Cytotoxicity

HepG2 (human liver carcinoma cells) and A549 (human alveolar adenocarcinoma basal epithelial cells) cell lines were obtained from the American Type Culture Collection (ATCC). Cells were cultured in Dulbecco's modified Eagle's medium (DMEM; Gibco, Invitrogen Corporation, USA) supplemented with 10% FBS (Natocor, Córdoba, Argentina) and antibiotics (100 U/ml penicillin and 100 μg/ml streptomycin; Gibco, Invitrogen Corporation, USA) in a humidified incubator at 37 °C under 5% CO_2 atmosphere. Cell viability was determined by the MTT assay [24]. A549 (4×10^3) and HepG2 (5×10^3) cells were seeded in a 96-well plate and incubated for 24 h under standard conditions. Then, the medium was discarded and replaced with different concentrations of blank SLN, free LN (dissolved in DMSO) or LN-loaded SLN in serum-free DMEM (final concentration of DMSO below 0.1%) for 24 h and 48 h. The medium was removed, and 100 μl of MTT solution (0.5 mg/ml MTT in supplemented DMEM medium) for 3 h. Later, the MTT solution was discarded, and the resulting formazan crystals were dissolved in 150 μl DMSO. The plates were shaken for 10 min, and the absorbance was read at 560 nm, and at 640 nm for background subtraction, in a microplate reader (Beckman Coulter DTX 880 Multimode Detector). Cell viability was expressed as a percentage of the untreated control (100% survival).

2.14. Cellular uptake

The cellular uptake of SLN was studied by incorporation of the green fluorescent dye DiOC18 (484/501 nm) to the nanoparticles. Briefly, 1.0 mg of the lipophilic tracer was mixed with the melted lipid phase (at 70 °C) until total dissolution and protected from light. The nanoparticles were prepared as previously described by addition of Pluronic F68 and sonication for 30 min at 50% potency. As a result, the dye was 100% encapsulated into the SLN.

The cellular uptake of fluorescent-labeled SLN was evaluated by fluorescence microscopy. A549 and HepG2 cells were plated onto cover slides of six-well plates at a density of 4×10^5 and 5×10^5 cells per well, respectively. After 24 h, cells were treated with serum-free DMEM containing 0.3 mg/ml SLN-MM-DiOC18 (0.75 μg/ml DiOC18) for 1, 2, 4, 8 and 24 h. After then, cells were washed three times with 2.0 ml PBS, fixed with paraformaldehyde 4.0% for 30 min at room temperature and mounted with ProLong® Gold Antifade Reagent with 4′,6-diamidino-2-phenylindole dihydrochloride (DAPI, 350/470 nm) for nuclear staining (Life Technologies, Carlsbad, CA, USA). Slides were examined under an Olympus BX51 fluorescence microscope (Tokyo, Japan) equipped with an Olympus DP70 digital camera, and the images were analyzed using ImagePro Plus v. 5.1 software (Media Cybernetics, Silver Spring, MD, USA).

2.15. Statistical analysis

Experimental data are expressed as the means ± SD. Statistical analysis was performed through the use of the one-way analysis of variance (ANOVA) and the Tukey–Kramer multiple-comparison test with the significance level set at $p < 0.05$ or the unpaired *t*-test.

3. Results

3.1. Linalool encapsulation into SLN

Encapsulation of LN into SLN was performed by dissolution of the monoterpene in the molten lipid phase and emulsification by the ultrasonication method [25]. The encapsulation efficiency was high for all tested formulations, reaching values of 92, 80 and 91% for SLN composed of MM, SS and CP, respectively (Table 1).

The potential changes in the initial EE of the SLN formulations due to crystallization of the lipid phase during storage were followed for one month at 5 °C. All the SLN-LN formulations were highly stable during the tested period and no significant changes in the EE values after 24 h, one week and 30 days ($p \geq 0.05$) were observed. These results suggest not only a good incorporation of LN into the lipid matrix, but also good stability by nanostructuration of the nanoparticles. The nanostructuration of SLN is based on the presence of the monoterpene phase that reduces the crystalline degree of the solid lipids [26]. The final LN concentrations were reported in Table 1 to be considered for further dilutions in citotoxicity assays.

Optical microscopy was used to detect the presence of nanoparticles after immediate preparation of the different SLN for-

Table 1
Encapsulation efficiency (EE) of Linalool in the different solid lipid nanoparticle formulations. Data are mean ± SD (n = 3).

SLN	Melting point* (°C)	EE(%)				Final LN concentration
		Initial	24 h	7 days	30 days	
MM	41	92.1 ± 8.1	93.6 ± 7.4	87.0 ± 7.5	94.8 ± 5.6	159.8 ± 6.5
SS	45	80.0 ± 8.0	82.3 ± 4.5	79.4 ± 6.2	81.7 ± 3.5	159.9 ± 7.7
CP	53	90.6 ± 5.6	87.7 ± 4.9	82.9 ± 5.8	92.8 ± 2.4	149.0 ± 2.8

*Of the pure lipid.

mulations. It was possible to observe the presence of nanoparticles as small dots in a narrow size distribution, confirming the development of a stable nanoemulsion (image not shown).

3.2. Nanoparticle morphology and size distribution

The SLN morphologies and size distributions were analyzed by TEM (Fig. 1). The SLN-MM formulation showed nanoparticles with a size smaller than 200 nm, and after the incorporation of LN, a significant decrease in size was observed. Furthermore, the presence of structures smaller than 50 nm, which can be produced by micelle formation between the surfactant and the non-encapsulated LN, was detected. A similar behavior was observed for the SLN-SS and SLN-CP formulations with the presence of nanoparticles mainly in the range of 100–200 nm and also a small fraction of nanoparticles with a diameter smaller than 50 nm. The SLN images showed spherical structure as expected for SLN systems.

In order to determine the size and distribution of the different SLN formulations, the mean particle size, polydispersity index (PDI) and zeta potential (Z pot) were analyzed by DLS (Table S1).

It was observed that the increase of the lipid melting point (MP) can be correlated with the increase in the mean diameter of nanoparticles under our experimental conditions data not shown). Also, the incorporation of LN into the SLN decreases SLN sizes by 22%, 27% and 21% for MM, SS and CP, respectively. Furthermore, a linear relationship between the increase in the lipid MP and the decrease in the PDI values was observed. A similar trend between the MP and the Z potential of nanoparticles was found (data not shown). Among the different formulations, SLN-MM exhibited the smallest diameter (118 nm and 92 nm for empty and LN-loaded SLN, respectively), but SLN-CP showed the lowest PDI values, indicating a narrow size distribution. In all cases, the incorporation of LN not only reduces the nanoparticle size but also the PDI values and the Z-potential (Table S1).

3.3. Physicochemical characterization of SLN-LN

The DSC curves of linalool, nanoparticles and LN-loaded SLN are displayed in Fig. 2. Linalool showed an intense endothermic peak at 159 °C, attributed to the decomposition and volatilization of monoterpene [27]. The DSC profile of SLN-MM exhibited two endothermic peaks at 38 °C and 45 °C, which correspond to the melting of the solid lipid [28]. Also, a degradation peak (exothermic) appeared at around 132 °C. The incorporation of LN into the lipid matrix produced some effects on the thermogravimetric behavior. A displacement of about 1–2 ° was observed in the first endothermic peaks, but the most relevant change was clearly seen in the exothermic peak, shifting the degradation process at 142 °C. SLN-SS nanoparticles showed smaller shifts after LN incorporation, and the main peak was endothermic and observed in the range of 46–48 °C, which can be attributed to the melting point of the pure raw material. In the case of SLN-CP an endothermic peak at 52 °C may result from the melting of the lipid matrix but no peak shift after LN incorporation was found. Besides, a slight shift in the degradation (exothermic) peak at 147 °C was observed. In all cases, the sharp endothermic peak was absent in the range of volatilization of pure LN, which can be explained considering the dissolution of LN in the molten lipid during encapsulation [25]. Also, the changes in lipid matrix after loading suggest modifications of the polymorphic state of the lipid from crystalline to amorphous, which may enhance the drug accommodation associated with high drug encapsulation [29].

TGA analysis was performed in order to visualize changes in the thermal properties of nanoparticles due to linalool incorporation (Figure S2 and Table S2).

LN suddenly began to degrade in the range of 32 °C to 150 °C, the decomposition ending at 250 °C. On the other hand, in the three SLN formulations (MM, SS and CP) the mass-loss event began at temperatures above 146 °C, 152 °C and 174 °C, respectively, following the trend observed in their respective melting points. The incorporation of LN clearly changed the thermal properties of SLN, indicating the presence of monoterpene dispersed into the lipid matrix. A reduction in the starting peak of mass loss temperature at 63 °C, 39 °C and 51 °C was observed for SLN MM-LN, SLN SS-LN and SLN CP-LN, respectively. These results indicate not only the effective encapsulation of LN into all SLN tested, but also suggest a reduction in the crystalline degree of nanoparticles, since the melting of substances in a less-ordered arrangement requires much less energy than the crystalline structures that need to overcome lattice forces [30].

The FTIR analysis of the samples was carried out to elucidate potential interactions between the cargo and the matrix (Fig. 3). Linalool showed absorption bands at 3410 cm^{-1}, 2974 cm^{-1} and 2930 cm^{-1}, which are attributed to the O—H stretching vibrations, the C—H stretching and the C—H aliphatic bands. Also, some peaks were observed at 1844 cm^{-1}, 1642 cm^{-1} (C=C stretching vibration of the allyl group), 1451 cm^{-1} and 1000 cm^{-1} (C—O stretching band) [27].

Solid lipid nanoparticles (SLN-MM, SLN-SS and SLN-CP) showed characteristic peaks in the range of 2915–2918 cm^{-1} and 2848–2849 cm^{-1} due to the ν_{aC-H} and ν_{sC-H} in CH2 vibration modes, respectively. Other bands related to the ester structures were observed in the region of 1731–1735 cm^{-1} ($\nu_{C=O}$ in ester); 1464–1466 cm-1 and 1342 cm-1 (δ_{C-H} in CH2) [25]. The band ranging from 1103 to 1114 cm^{-1} could be assigned to the ν_{C-O-C} stretching vibrations of $-OCH_2CH_2$ residues repeated along the Pluronic F68 structure [31].

The IR spectrum of LN-loaded SLN was also determined. For SLN-MM-LN formulation, a shift of 4 cm^{-1} was observed for the peak related to the δ_{C-H} in $-CH_2$ of the ester structure (1464 cm^{-1}) and another shift of 9 cm^{-1} for the band associated with the structure of Pluronic F68 (C—O—C stretching vibrations at 1103 cm^{-1}). SLN-SS-LN also exhibited a displacement (5 cm^{-1}) in the peak at 1106 cm^{-1} (due to Pluronic vibrations) in addition to a strong shift in the band associated with the O—H stretching vibrations (at 3361 cm^{-1}). On the other hand, LN-loaded SLN—CP nanoparticles showed a shift of 5 cm^{-1} in the peak of Pluronic (at 1114 cm^{-1}) and of 6 cm^{-1} in the band at 2918 cm^{-1} (ν_{aC-H}). Other smaller peak shifts (from 1 to 3 cm^{-1}) were observed after LN incorporation, suggesting the presence of weak interactions between LN and the lipid matrixes, possibly by the formation of hydrogen bonds and/or hydrophobic interactions. The displacement in the Pluronic F68

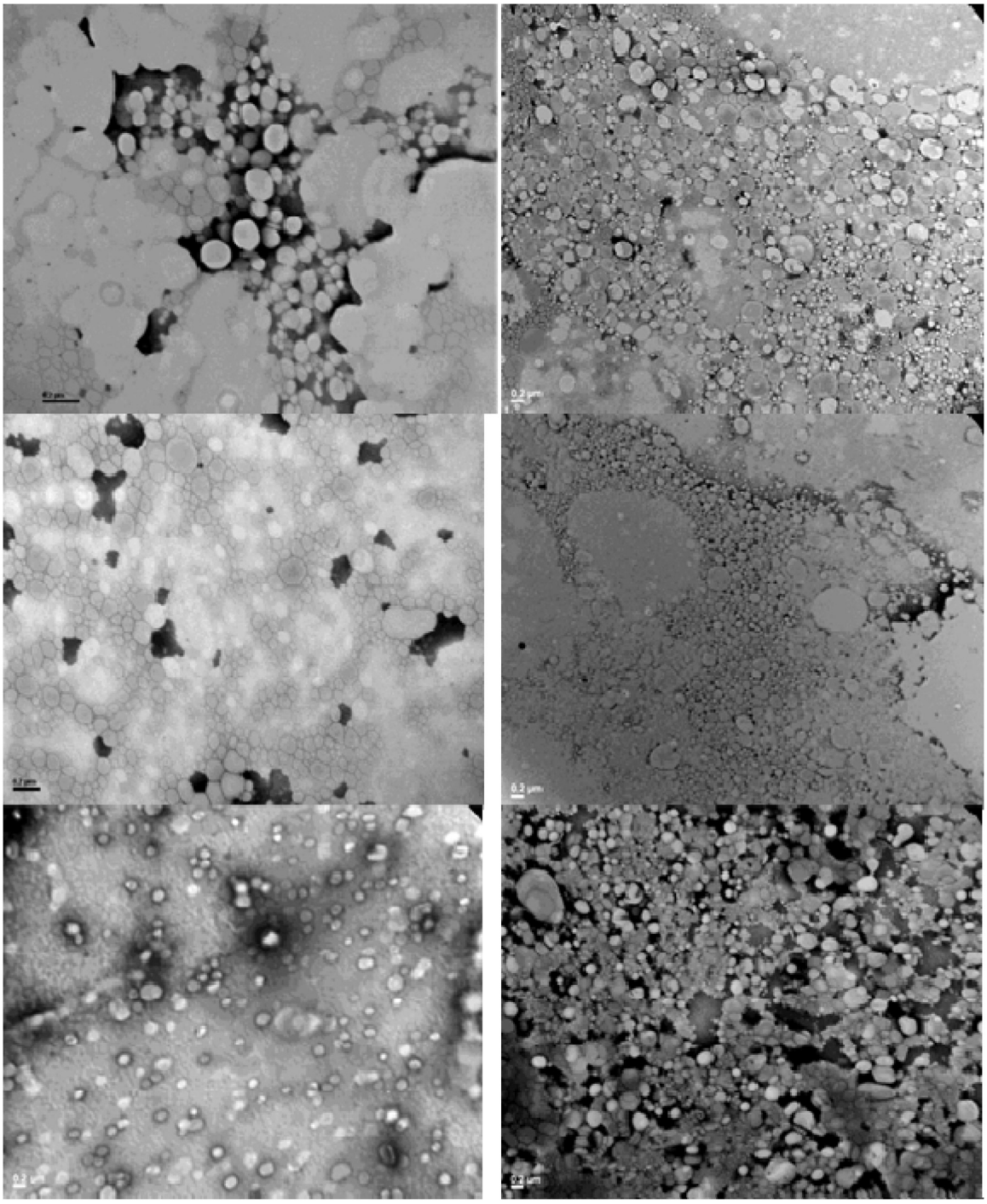

Fig. 1. TEM images of MM, SS and CP SLNs: empty (left) and LN loaded (right).

band (mainly located at the surface) could be due to the presence of non-encapsulated LN that forms micelles with the surfactant [32].

The X-ray diffraction technique was employed to confirm the solid crystalline structure of SLN and to identify the polymorphism of the lipid matrix after preparation and LN incorporation (Fig. S3). It was previously established that fats can crystallize in three main polymorphic forms, in which the α form is unstable, the β is the most stable, and the βí is a metastable form that still possesses disorder regions and maintains a partial amorphous state [33]. The solid lipid nanoparticles of different lipid nature (MM, SS and CP) prepared by the sonication method showed a mixture of polymorphs, displaying characteristic short spacing at 0.46/0.38/0.37 nm (typical of the β modification) and 0.42/0.38 nm (βí form) [34]. The SLN of MM exhibited sharp peaks at 2&z.Theta; scattered angles of 19.1°, 20.7°, 21.6°, 23.3° and 23.9°, confirming the lipid crystalline nature. The incorporation of LN produced slight changes in those peaks, but the absence of the peak at 20.7° suggests the modification of the crystal structure due to a less ordered matrix. In the case of SLN-SS, a similar pattern was observed with peaks at 19.1°, 21.4°, 23.3° and 23.6° for empty nanoparticles, but the last two peaks fused when LN was encapsulated, which suggests a predominance of the βí architecture. Finally, the SLN-CP diffraction pattern displayed the same typical structure, with peaks at 19.1°, 21.6°, 23.3°, and a weak peak at 23.8°. After LN incorpora-

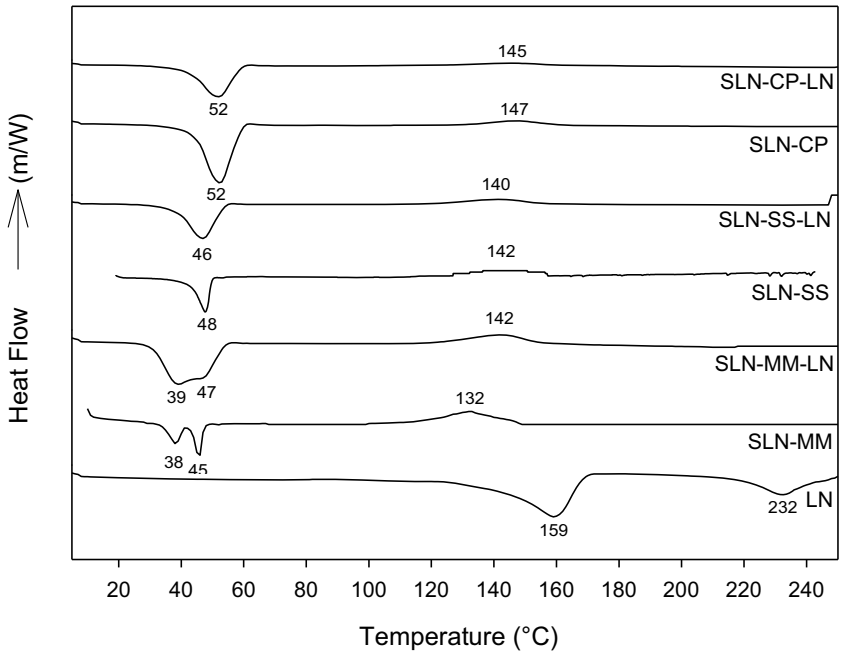

Fig. 2. Thermogravimetric curves of Linalool (LN), solid lipid nanoparticles (SLN) and LN loaded SLN.

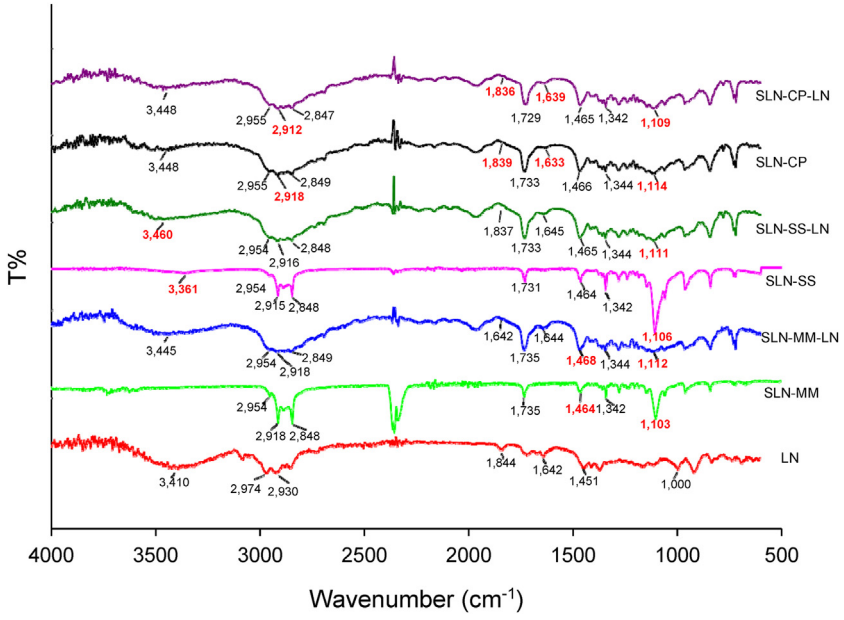

Fig. 3. FTIR analysis of Linalool (LN), solid lipid nanoparticles (SLN) and LN loaded SLN.

tion, the same peaks were observed, but the intensity of the peak at 23.8° increased, indicating a transition from the metastable form (βí) to the more stable β polymorphism. However, this transition was incomplete since the peak at 0.42 nm still remained detectable.

The observed patterns were characteristic of complex triglyceride mixtures showing different polymorphic forms in the same sample [35]. It is important to establish the crystalline structure of lipid nanoparticles since the release properties of the encapsulated drugs and the stability during storage are significantly influenced. Particularly, complete transitions from β′ to β forms indicate a higher crystal order packing, and hence could lead to a not desirable faster drug expulsion [36].

3.4. Release studies of LN from SLN

The release profiles of LN from the SLN formulations were evaluated at neutral pH and 37 °C, simulating the physiological media of the body (Fig. 4). SLN containing LN showed a biphasic behavior with a fast initial release during the first 6 h, followed by a slow release afterwards. In all cases, the LN controlled release profiles remained for at least 72 h (Fig. 4).

One of the factors contributing to the initial fast release could be attributed to the presence of free LN (non-entrapped) that could be solubilized by the surfactant micelles. Another factor could be the location of encapsulated LN near the surface of nanoparticles. Results also suggest a nanostructuration of the matrix due to the

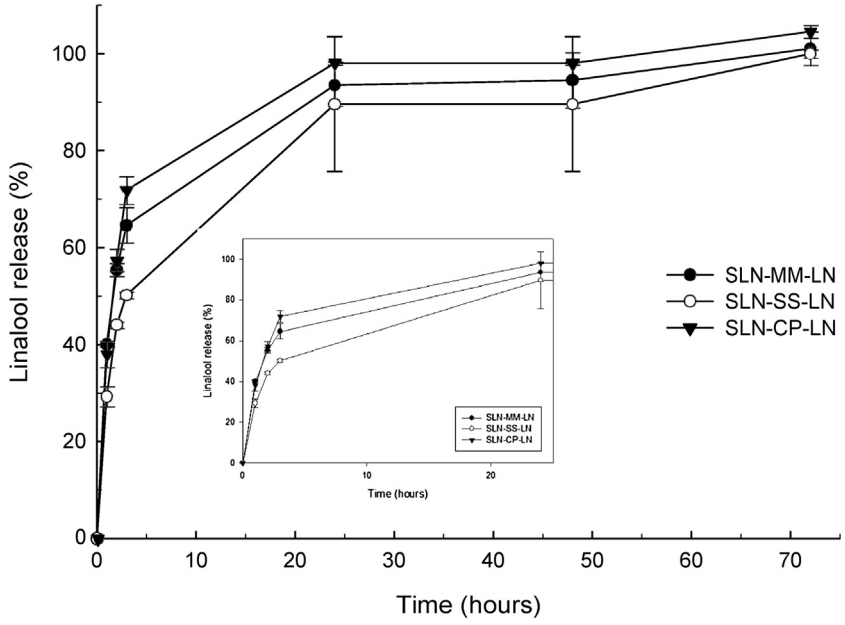

Fig. 4. Release profile of LN from SLN formulations at pH 7.4. The experimental values are the mean ± SD, n = 3).

incorporation of monoterpene. The presence of liquid lipids within the solid lipid produced an imperfect crystal lattice, causing high mobility of the loaded molecules and subsequently increasing the drug diffusion outside the nanoparticle [26].

3.5. Cytotoxicity assay

In order to analyze the potential benefits of LN encapsulation, the antiproliferative activity of free and linalool-loaded SLN was evaluated on two different cancer cell lines (HepG2 and A549 cells). Cells were treated with a range of LN concentrations (0.5–2.0 mM) for 24 and 48 h based on results obtained previously [11]. First, cell survival was assessed in the presence of the different formulations of unloaded SLN at different concentrations (0.15–0.30 mg/ml) equivalent to those for SLN-LN (1.0–2.0 mM LN). It was observed that cell viability was affected depending on the nature of the lipid matrix. Meanwhile, the myristyl myristate and cetyl ester based nanoparticles showed no toxicity in the range of concentrations evaluated, but those synthesized with cetyl palmitate resulted cytotoxic in both cell lines (Table 2). The cytotoxicity results for SLN-CP are in agreement with previous reports elsewhere for other cell lines [37,38]. The MTT assay showed that free LN, as expected, as well as SLN-MM-LN and SLN-SS-LN suppressed HepG2 and A549 cell proliferation in a concentration- and time-dependent manner. However, no differences in cell survival were observed between LN-loaded and unloaded SLN at concentrations up to 1.0 mM (Fig. 5).

In A549 cells, only SLN-MM-LN exhibited higher cytotoxicity than free LN. This phenomenon was observed at 1.5 and 2.0 mM, and potentiated in a time-dependent manner, significantly enhancing antitumoral activity between 11% and 15% (Fig. 5**a**). On the other hand, both SLN-MM-LN and SLN-SS-LN improved the inhibitory efficiency of free LN in HepG2 cells. The most outstanding results were observed for SLN-MM-LN (2.0 mM, 48 h), where LN-loaded nanoparticles showed stronger anticancer activity than free LN, inhibiting cell growth by 76% rather than by 43% as in the last one ($p = 0.0005$) (Fig. 5**b**).

3.6. Cellular uptake of SLN

In order to evaluate the cellular uptake, the highly hydrophobic fluorescent probe DiOC18 was selected for labeling myristyl myristate SLN. The fluorescent probe was 100% encapsulated, and no release was observed under the experimental conditions tested (data not shown). HepG2 cells and A549 cells were incubated with labeled SLN for 1, 2, 4, 8 and 24 h and analyzed by fluorescence microscopy (Fig. 6).

Table 2
Cytotoxicity of empty SLN formulations. Data are expressed as the means ± SD (n = 3). Significant differences at $p < 0.05$ (*), $p < 0.01$ (**), $p < 0.001$ (***) levels vs. control untreated cells (ANOVA test).

SLN formulation	Concentration (mg/ml)2.1.2.4 2.1.2.4	Cell viability (%)			
		HepG2		A549	
		24 h	48 h	24 h	48 h
MM	0.15	114.7 ± 13.8	130.0 ± 11.7*	101.7 ±7.4	101.0 ± 4.8
	0.23	103.1 ± 8.1	120.3 ± 13.9	115.4 ±7.0	103.5 ± 5.1
	0.30	114.9 ± 6.8	111.7 ± 10.6	114.5 ± 7.6	98.3 ± 2.5
CP	0.15	59.9 ± 7.4**	78.9 ± 7.5**	84.6 ± 10.0	81.4 ± 7.3*
	0.23	52.1 ± 7.9***	66.9 ± 12.6**	65.1 ± 8.4**	72.4 ± 7.7**
	0.30	58.7 ± 8.5**	71.5 ± 3.7***	53.7 ± 5.2**	66.9 ± 5.1**
SS	0.15	123.6 ± 16.6	120.7 ± 11.4*	110.7 ± 12.0	99.3 ± 4.8
	0.23	113.4 ± 21.2	124.5 ± 9.3**	105.7 ± 10.3	92.6 ± 6.1
	0.30	118.8 ± 14.6	121.8 ± 7.7**	110.6 ± 5.9	102.7 ± 9.5

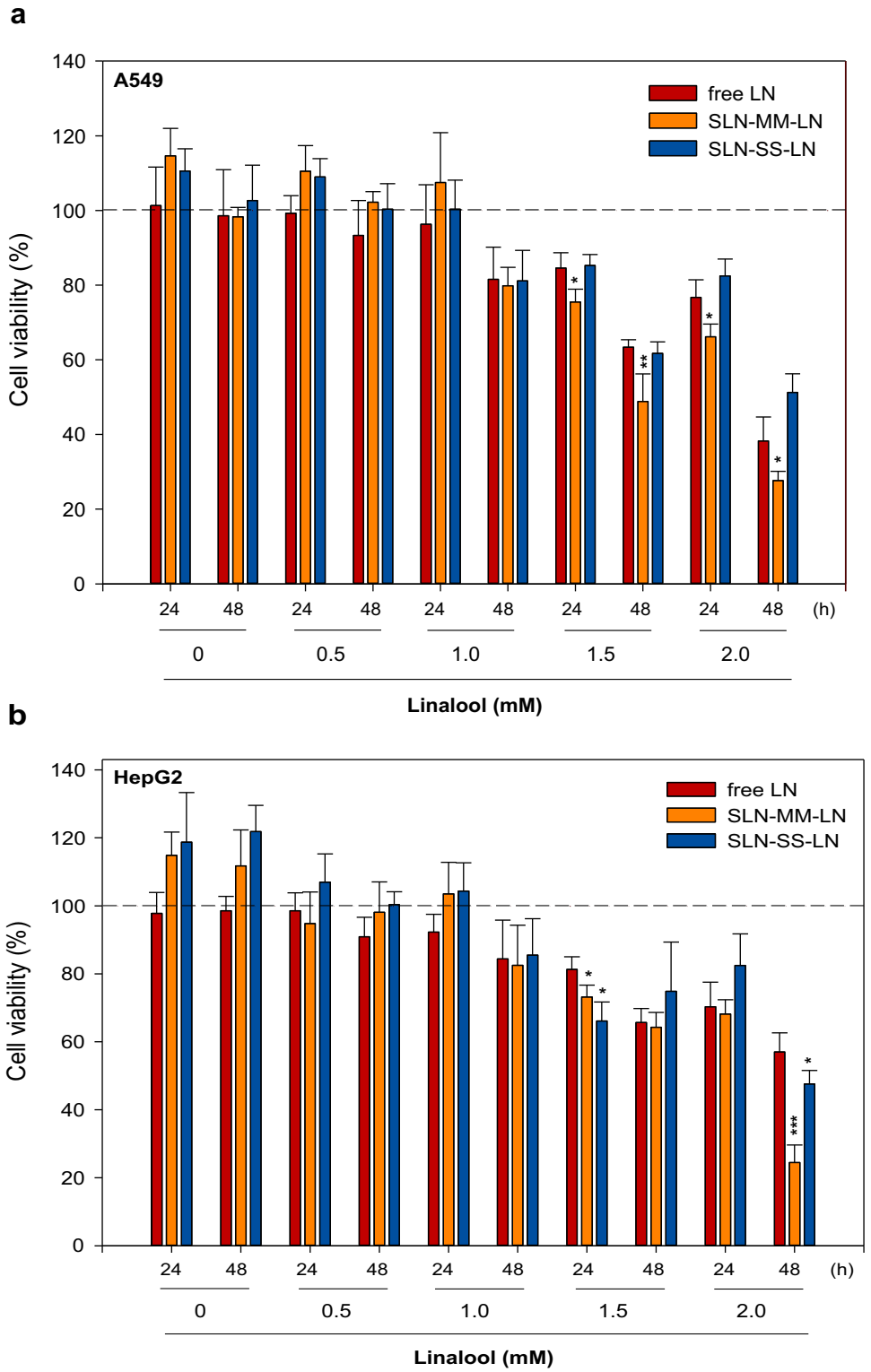

Fig. 5. Cytotoxicity assay of LN-loaded SLN formulations in HepG2 and A549 cells. Concentration-dependent cytotoxicity of free and loaded-SLN linalool in HepG2 (a) and A549 (b) cells for 24 h and 48 h. The control bars for the blank SLN formulations correspond to the maximum concentration evaluated (0.3 mg/ml). Data are expressed as the means ± SD of three independent experiments performed in at least triplicate; (*) $p < 0.05$, (**) $p < 0.01$, (***) $p < 0.001$ vs. the same treatment with free linalool.

The cellular uptake of SLN occurs in a time-dependent manner. As was also observed in living cells under inverted florescence microscope (data not shown), the fluorescence signal began to be detectable after 1 h incubation in A549 cells, and SLN penetration kinetics was evident in time, reaching a maximum at 8 h, when the green signal was predominantly cytoplasmic (Fig. 6**a**). A similar behavior was noticed for HepG2 cells, but in this case, the fluorescent label was slightly evident after 2 h treatment, and the maximum intensity was reached after 24 h (Fig. 6**b**). This is a very interesting result since it demonstrates the ability of SLN to penetrate into the cell and transport the loaded drug to the cytoplasm region similarly as previously reported [39]. It also reveals differ-

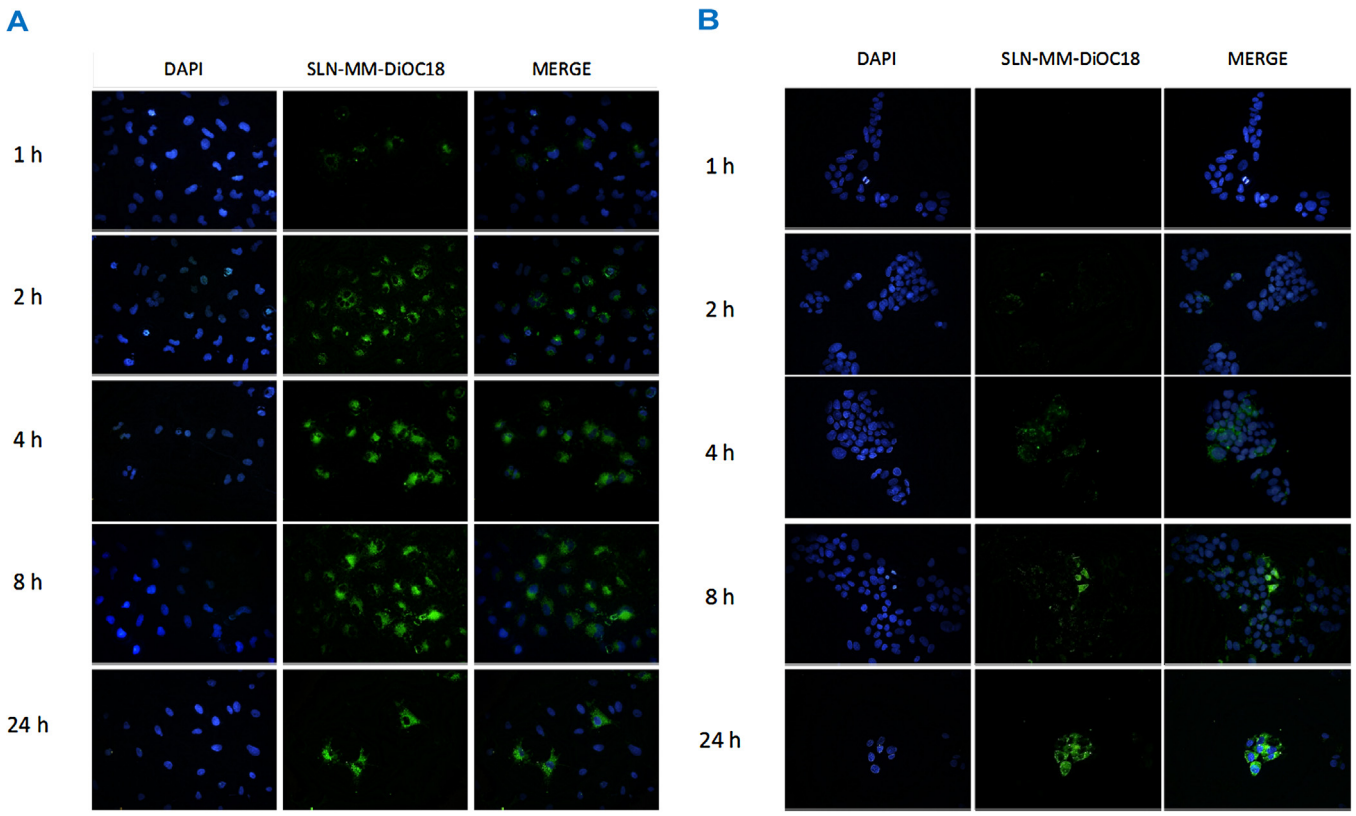

Fig. 6. Cellular uptake of DiOC18- loaded myristyl myristate SLN in A549 (a) and HepG2 (b) cells. Fluorescence microscopy was used to monitor the cellular uptake of labeled nanoparticles (green) at different time points (1–24 h). Nuclei were stained with 4,6-diamino-2-phenylindole DAPI (blue). Representative images of triplicate experiments are shown. Magnification 600×. (For interpretation of the references to colour in this figure legend, the reader is referred to the web version of this article.)

ences in the metabolism of each cell type, since the incorporation of SLN by A549 cells was faster than in HepG2 and it was in concordance with the cell proliferation rate commonly found for these cell lines [4,11,12].

4. Conclusions

High encapsulation of LN into solid lipid nanoparticles was successfully achieved in three different formulations: MM, SS and CP matrices, which becomes an interesting approach to improve the bioavailability of monoterpene and also avoid the use of toxic vehicles such as DMSO. Nanoparticles with a mean size around 100 nm and a narrow size distribution were able to release LN in a controlled release manner. The formulations were stable for at least 30 days kept at 5 °C and protected from light.

The physicochemical analysis revealed the good incorporation of LN into the lipid carriers, and weak interactions between the components were established, changing the thermal and structural properties of empty lipid nanoparticles. The results suggest a nanostructuration of the SLN after LN incorporation due to the properties of the natural isoprenoid in the matrix crystal structure.

The cytotoxic effect of LN on human lung- and liver-derived tumor cells (A549 and HepG2, respectively) was exacerbated when it was incorporated into SLN at concentrations higher than 1.0 mM in a dose/time manner. This is an interesting approach to enhance the antitumoral activity of novel or common drugs currently used in cancer therapy. In addition, to potentiate the therapeutic treatments while reducing the undesirable side effects, combined encapsulation with monoterpenes and conventional drugs is under study.

Finally, the present study demonstrates the uptake of the developed nanoparticles to be intracellular and opens the gate to explore new synergistic effects by delivering hydrophobic drugs, (*e.g.*, some anticancer drugs) into SLN in an efficient manner.

Acknowledgements

The present work was supported by Argentine grants from CONICET (National Council for Science and Technology, PIP 0498), The National Agency of Scientific and Technological Promotion (ANPCyT, PICT 2011-2116), UNLP (National University of La Plata, 11/X701 and PRH 5.2). Dr. G.A. Islan wants to thank the "Subsidio para jóvenes investigadores UNLP 2014" and the "Premio a la innovación UNLP 2014". Also, we want to thank CRODA Argentina for kindly donating the lipids. Support from the Brazilian Network on Nanotoxicology (MCTI/CNPq) and NanoBioss (MCTI)-Brazil is also acknowledged. We also want to thank Dr. Mauricio Di Ianni, Dr. Pablo Cortez Tornello, Dr. Ignacio Pérez de Verti and Dr. Gustavo Morel for DLS, TGA/XRD, FTIR, and fluorescence microscopies.

Appendix A. Supplementary data

Supplementary data associated with this article can be found, in the online version, at http://dx.doi.org/10.1016/j.colsurfb.2017.03.021.

References

[1] Who, World Health Statistics 2008, World Health Organization, 2008.
[2] G.M. Cragg, D.J. Newman, Plants as a source of anti-cancer agents, J. Ethnopharmacol. 100 (2005) 72–79.
[3] S. Nair, W. Li, A.N. Kong, Natural dietary anti-cancer chemopreventive compounds: redox-mediated differential signaling mechanisms in cytoprotection of normal cells versus cytotoxicity in tumor cells, Acta Pharmacol. Sin. 28 (2007) 459–472.

[4] S. Jana, K. Patra, S. Sarkar, J. Jana, G. Mukherjee, S. Bhattacharjee, D.P. Mandal, Antitumorigenic potential of linalool is accompanied by modulation of oxidative stress: an in vivo study in sarcoma-180 solid tumor model, Nutr. Cancer 66 (2014) 835–848.
[5] A. Lapczynski, S.P. Bhatia, C.S. Letizia, A.M. Api, Fragrance material review on l-linalool, Food Chem. Toxicol. 46 (Suppl. 11) (2008) S195–196.
[6] A.C. Aprotosoaie, M. Hăncianu, I.I. Costache, A. Miron, Linalool: a review on a key odorant molecule with valuable biological properties, Flavour Frag. J. 29 (2014) 193–219.
[7] Y. Li, O. Lv, F. Zhou, Q. Li, Z. Wu, Y. Zheng, Linalool inhibits LPS-induced inflammation in BV2 microglia cells by activating Nrf2, Neurochem. Res. 40 (2015) 1520–1525.
[8] G.H. Seol, P. Kang, H.S. Lee, G.H. Seol, Antioxidant activity of linalool in patients with carpal tunnel syndrome, BMC Neurol. 16 (2016) 17.
[9] S. Mehri, M.A. Meshki, H. Hosseinzadeh, Linalool as a neuroprotective agent against acrylamide-induced neurotoxicity in Wistar rats, Drug Chem. Toxicol. 38 (2015) 162–166.
[10] S.N. Park, Y.K. Lim, M.O. Freire, E. Cho, D. Jin, J.K. Kook, Antimicrobial effect of linalool and alpha-terpineol against periodontopathic and cariogenic bacteria, Anaerobe 18 (2012) 369–372.
[11] B. Rodenak Kladniew, M. Polo, S. Montero Villegas, M. Galle, R. Crespo, M. Garcia de Bravo, Synergistic antiproliferative and anticholesterogenic effects of linalool, 1, 8-cineole, and simvastatin on human cell lines, Chem. Biol. Interact. 214 (2014) 57–68.
[12] Y. Gu, Z. Ting, X. Qiu, X. Zhang, X. Gan, Y. Fang, X. Xu, R. Xu, Linalool preferentially induces robust apoptosis of a variety of leukemia cells via upregulating p53 and cyclin-dependent kinase inhibitors, Toxicology 268 (2010) 19–24.
[13] R. Ravizza, M.B. Gariboldi, R. Molteni, E. Monti, Linalool, a plant-derived monoterpene alcohol, reverses doxorubicin resistance in human breast adenocarcinoma cells, Oncol. Rep. 20 (2008) 625–630.
[14] R. Zenhausern, A. Tobler, L. Leoncini, O.M. Hess, P. Ferrari, Fatal cardiac arrhythmia after infusion of dimethyl sulfoxide-cryopreserved hematopoietic stem cells in a patient with severe primary cardiac amyloidosis and end-stage renal failure, Ann. Hematol. 79 (2000) 523–526.
[15] F. Shi, Y. Zhao, C.K. Firempong, X. Xu, Preparation, characterization and pharmacokinetic studies of linalool-loaded nanostructured lipid carriers, Pharm. Biol. (2016) 1–9.
[16] D. Paolino, D. Cosco, F. Cilurzo, M. Fresta, Innovative drug delivery systems for the administration of natural compounds, Curr. Bioact. Compd. 3 (2007) 262–277.
[17] R.H. Muller, K. Mader, S. Gohla, Solid lipid nanoparticles (SLN) for controlled drug delivery – a review of the state of the art, Eur. J. Pharm. Biopharm. 50 (2000) 161–177.
[18] J.S. Baek, C.W. Cho, Controlled release and reversal of multidrug resistance by co-encapsulation of paclitaxel and verapamil in solid lipid nanoparticles, Int. J. Pharm. 478 (2015) 617–624.
[19] A.Z. Wilczewska, K. Niemirowicz, K.H. Markiewicz, H. Car, Nanoparticles as drug delivery systems, Pharmacol. Rep. 64 (2012) 1020–1037.
[20] W. Mehnert, K. Mader, Solid lipid nanoparticles: production, characterization and applications, Adv. Drug Deliv. Rev. 47 (2001) 165–196.
[21] V. Venkateswarlu, K. Manjunath, Preparation, characterization and in vitro release kinetics of clozapine solid lipid nanoparticles, J. Control. Release 95 (2004) 627–638.
[22] D. Martins, L. Frungillo, M.C. Anazzetti, P.S. Melo, N. Duran, Antitumoral activity of L-ascorbic acid-poly-D,L-(lactide-co-glycolide) nanoparticles containing violacein, Int, J. Nanomed. 5 (2010) 77–85.
[23] D. Palmer, M. Levina, T.P. Farrell, A.R. Rajabi-Siahboomi, The influence of hydro-alcoholic media on drug release, Pharm. Technol. 35 (2011) 50–58.
[24] T. Mosmann, Rapid colorimetric assay for cellular growth and survival: application to proliferation and cytotoxicity assays, J. Immunol. Met. 65 (1983) 55–63.
[25] G.A. Islan, P.C. Tornello, G.A. Abraham, N. Duran, G.R. Castro, Smart lipid nanoparticles containing levofloxacin and DNase for lung delivery, Des. Charact. Colloid. Surf. B 143 (2016) 168–176.
[26] C.L. Fang, S.A. Al-Suwayeh, J.Y. Fang, Nanostructured lipid carriers (NLCs) for drug delivery and targeting, Rec. Pat. Nanotechnol. 7 (2013) 41–55.
[27] P. Menezes, M. Serafini, L. Quintans-Júnior, G. Silva, J. Oliveira, F. Carvalho, J. Souza, J. Matos, P. Alves, I. Matos, Inclusion complex of (−)-linalool and β-cyclodextrin, J. Therm. Anal. Calorim. 115 (2014) 2429–2437.
[28] V. Sanna, G. Caria, A. Mariani, Effect of lipid nanoparticles containing fatty alcohols having different chain length on the ex vivo skin permeability of Econazole nitrate, Powder Technol. 201 (2010) 32–36.
[29] A.C. Vieira, L.L. Chaves, M. Pinheiro, D. Ferreira, B. Sarmento, S. Reis, Design and statistical modeling of mannose-decorated dapsone-containing nanoparticles as a strategy of targeting intestinal M-cells, Int. J. Nanomed. 11 (2016) 2601–2617.
[30] E.D.P. Almeida, A.A. Costa, M.R. Serafini, F.C. Rossetti, J.M. Marchetti, V.H.V. Sarmento, R.S. de Nunes, M.E.G. Valerio, A.A. Araújo, A.A.M. Lira, Preparation and characterization of chloroaluminum phthalocyanine-loaded solid lipid nanoparticles by thermal analysis and powder X-ray diffraction techniques, J. Therm. Anal. Calorim. 108 (2011) 191–196.
[31] T. Wang, Y. Wu, A.J. Zeng, Synthesis and characterization of amphiphilic pluronic (F68)-1, 2-dipalmitoyl-sn-glycero-3-phosphoethanolamine copolymers and their micelles as a drug carrier, J. Appl. Pol. Sci. 117 (2010) 604–613.
[32] D.L. Berthier, I. Schmidt, W. Fieber, C. Schatz, A. Furrer, K. Wong, S. Lecommandoux, Controlled release of volatile fragrance molecules from PEO-b-PPO-b-PEO block copolymer micelles in ethanol-water mixtures, Langmuir 26 (2010) 7953–7961.
[33] H. Bunjes, T. Unruh, Characterization of lipid nanoparticles by differential scanning calorimetry, X-ray and neutron scattering, Adv. Drug Deliv. Rev. 59 (2007) 379–402.
[34] J. Yang, O.N. Ciftci, Formation of hollow solid lipid micro-and nanoparticles using supercritical carbon dioxide, Food Bioprod. Process. 98 (2016) 151–160.
[35] R. Shah, D. Eldridge, E. Palombo, I. Harding, Lipid Nanoparticles: Production, Characterization and Stability, Springer, New York, 2015.
[36] V. Jenning, M. Schafer-Korting, S. Gohla, Vitamin A-loaded solid lipid nanoparticles for topical use: drug release properties, J. Control. Release 66 (2000) 115–126.
[37] D.M. Ridolfi, P.D. Marcato, D. Machado, R.A. Silva, G.Z. Justo, N. Durán, In vitro cytotoxicity assays of solid lipid nanoparticles in epithelial and dermal cells, J. Phys.: Conf. Series (2011) 012032.
[38] S. Martins, S. Costa-Lima, T. Carneiro, A. Cordeiro-da-Silva, E.B. Souto, D.C. Ferreira, Solid lipid nanoparticles as intracellular drug transporters: an investigation of the uptake mechanism and pathway, Int. J. Pharm. 430 (2012) 216–227.
[39] S. Scalia, V. Trotta, D. Traini, P.M. Young, C. Sticozzi, F. Cervellati, G. Valacchi, Incorporation of quercetin in respirable lipid microparticles: effect on stability and cellular uptake on A549 pulmonary alveolar epithelial cells, Colloids Surf. B 112 (2013) 322–329.